Chemical Engineering Journal 281 (2015) 771–781

Contents lists available at ScienceDirect

Chemical Engineering Journal

journal homepage: www.elsevier.com/locate/cej

Preparation of graphene oxide/dendrimer hybrid carriers for delivery of doxorubicin

Ampornphan Siriviriyanun [a], Marina Popova [b], Toyoko Imae [a,b,*], Lik Voon Kiew [c], Chung Yeng Looi [c], Won Fen Wong [d], Hong Boon Lee [e], Lip Yong Chung [e,*]

[a] Graduate Institute of Applied Science and Technology, National Taiwan University of Science and Technology, 43 Section 4, Keelung Road, Taipei 10607, Taiwan, ROC
[b] Department of Chemical Engineering, National Taiwan University of Science and Technology, 43 Section 4, Keelung Road, Taipei 10607, Taiwan, ROC
[c] Department of Pharmacology, Faculty of Medicine, University of Malaya, 50603 Kuala Lumpur, Malaysia
[d] Department of Medical Microbiology, Faculty of Medicine, University of Malaya, 50603 Kuala Lumpur, Malaysia
[e] Department of Pharmacy, Faculty of Medicine, University of Malaya, 50603 Kuala Lumpur, Malaysia

HIGHLIGHTS

- Graphene oxide (GO) carriers are hybridized with dendrimer and folic acid.
- Small hybrid carrier possesses a loading capacity of 1.43 g/g(GO) for doxorubicin.
- The considerable amounts (86%) of loaded drug are released at pH 5.5 after 72 h.
- The hybrid carrier reveals the efficient intracellular uptake in the HeLa cells.
- This hybrid is a potential candidate of nanocarriers for anticancer drugs.

GRAPHICAL ABSTRACT

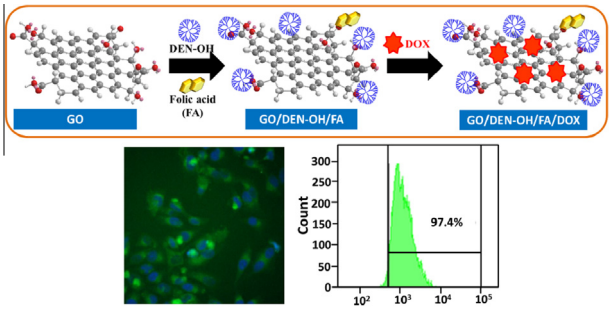

ARTICLE INFO

Article history:
Received 8 April 2015
Received in revised form 10 June 2015
Accepted 6 July 2015
Available online 10 July 2015

Keywords:
Graphene oxide
OH-terminated poly(amido amine) dendrimer
Folic acid
Doxorubicin
Drug loading/releasing

ABSTRACT

Hybrid carriers were successfully synthesized by chemically binding OH-terminated fourth generation poly(amido amine) dendrimer and folic acid on graphene oxide (GO) with a size of 100 nm, and their drug carrier ability was compared with hybrids of 1500 nm GO. The small hybrid carriers possessed a 1.3 times lower loading capacity (1.43 g/g(GO)) for doxorubicin (DOX) than the large hybrid carriers. However, the amount (86%) of DOX released at pH 5.5 from the small hybrids after 72 h was 1.14 times larger than from the large hybrids. This difference could be due to the extent of π–π interaction between DOX and the graphitic domain on GO. In vitro MTT assays revealed that the small hybrids led to higher cell viability than 63% at 0.75 μg/ml in HeLa human cervical cancer cells. An investigation of the intracellular uptake of hybrid carriers revealed the efficient internalization of small hybrids in the HeLa cells (97% at 62.5 mg/ml). Taken together, these results indicate that the small hybrids consisting of 100 nm GO carrier can successfully load and deliver the anticancer drug DOX into HeLa cells. In the carriers, dendrimer had a role of stable suspension of the hybrids in water, and folic acid acted as an effective anchoring of the hybrids on HeLa cells. The present investigation highlights the potential use of these hybrid materials as nanocarriers with high loading and releasing efficiency for the delivery of anticancer drugs to tumor cells.

* Corresponding authors at: Graduate Institute of Applied Science and Technology, National Taiwan University of Science and Technology, Taipei 10607, Taiwan, ROC (T. Imae).
E-mail addresses: imae@mail.ntust.edu.tw (T. Imae), chungly@hotmail.com (L.Y. Chung).

http://dx.doi.org/10.1016/j.cej.2015.07.024
1385-8947/

1. Introduction

Targetable drug nanocarriers have been developed to achieve highly selective delivery of anticancer drugs to tumor cells in a controlled-release fashion [1–8]. Graphene oxide (GO) is an oxidized graphene composed of a graphitic sheet, which is chemically functionalized with oxygen-including groups such as hydroxyl, carboxyl, carbonyl and epoxide [9]. Due to its biocompatibility [10], many researchers have focused on the potential of using GO and its derivatives as a promising new material for biomedical applications [3–8]. In particular, GO has been considered to be a potential carrier for drug delivery system, because the 2D sheet of GO has a large surface area. As a result, drugs can be loaded onto both sides of the graphene sheet through π–π stacking, covalent binding, and hydrophobic or electrostatic interaction [4,11]. Folic acid (FA)-conjugated nano-GO (FA-nano-GO) has been shown to specifically target human MCF–7 breast cancer cells that express the folate receptor [4]. Furthermore, the successively controlled loading of two anticancer drugs, doxorubicin (DOX) and camptothecin (CPT), onto FA-nano-GO has been achieved via π–π stacking and hydrophobic interactions.

In addition to these properties, the functionalization of GO with biodegradable, biocompatible, nonimmunogenic and water-soluble polymers, such as poly(amido amine) (PAMAM) dendrimers, could further enhance the utility of GO nanohybrid materials as nanocarriers in drug delivery systems [12–14]. Because low-generation (G1–G4) PAMAM dendrimers can be electrostatically associated with lipid membranes and amphiphilic bilayers [15,16], the immobilization of PAMAM dendrimers onto GO may help GO hybrids to bind tightly on cell membranes. In addition, the cellular uptake of dendrimer–based drug delivery systems has been proven to be significantly higher than the linear polymeric carriers, which can be attributed to the nanosize and the compact, spherical geometry of dendrimers [17]. Thus, it is imperative to modify GO with dendrimers to achieve effective drug loading ability and, consequently, efficient drug delivery.

In the present study, the advanced nanocarriers for drug delivery systems were developed by protecting GO with water-soluble PAMAM dendrimers. Hydroxyl–terminated PAMAM dendrimers (DEN-OH) were selected, because compounds with amine-terminals are rather toxic [18]. FA was also bound onto GO to target the nanocarriers to specific cells including HeLa cells [19]. Then, in addition to a comparative study of the size dependence of the GO/DEN-OH/FA carriers, the carriers were assessed their ability to load and release doses of DOX and were also evaluated their effects on the viability and the intracellular uptake efficiency by HeLa cells.

2. Experimental section

2.1. Materials and characterizations

An aqueous dispersion of GO (0.275 mg/cm^3) with an average particle size of 1500 nm was purchased from UniRegion Bio-Tech, USA. DEN-OH (10 wt% in methanol) was purchased from Aldrich Chemical Co. N-hydroxysuccinimide (NHS), 4-dimethylaminopyridine (DMAP), N,N′-dicyclohexylcarbodiimide (DCC), dimethylformamide (DMF), FA, 1-[3-(dimethylamino)propyl]-3-ethylcarbodiimide hydrochloride (EDC), sodium hydrogen carbonate ($NaHCO_3$), and dimethylsulfoxide (DMSO) were purchased from ACROS, USA. Ultrapure (Millipore Milli-Q) water with a resistivity of 18.2 MΩcm was used throughout all syntheses and measurements. Dulbecco's modified Eagle's medium (DMEM), penicillin streptomycin (PS), fetal bovine serum (FBS), sodium pyruvate and L-glutamine were purchased from GIBCO, Brazil. 3-(4,5-Dimethylthiazol-2-yl)-2,5-diphenyl tetrazolium bromide (MTT) and fluoresceinyl glycine amide (FGA) were purchased from Sigma. HeLa cells and DOX were kindly donated by Prof. H. C. Tsai, National Taiwan University of Science and Technology, Taiwan.

Sonication was performed on an ultrasonic processor (QSONICA, Sonicator Q700) with a ½" horn tip. Dynamic light scattering (DLS) and zeta potential measurements were performed on a nanoparticle analyzer (Horiba, SZ-100) with diode-pumped solid-state laser (DPSS laser, 532 nm). Infrared (IR) absorption spectra were recorded with KBr pellets of sample powders on an FTIR spectrometer (Nicolet, Nexus 670). Ultra violet–visible–near infrared (UV–VIS–NIR) absorption spectroscopic measurements were performed on a Jasco V-670 series UV spectrometer with a 1 mm quartz cell. Fluorescence was measured with a HITACHI F-3010 fluorometer at a scan rate of 30 nm/min using a 10 mm quartz cell. The specimens for UV–VIS–NIR absorption and fluorescence spectra were suspensions of sample powders in water under sonication. Transmission electron microscopic (TEM) images were taken by a Hitachi H-7000 instrument, operated at 100 kV. Atomic force microscopic (AFM) observation was performed in air using a Digital Instruments NanoScope III apparatus. Freshly cleaved mica was used as a substrate. The sample suspensions were spin-coated onto the mica surface and then dried in air. Thereafter, the specimens were immediately subjected to AFM analysis using a contact mode with a scan rate of 0.99 Hz and a tip velocity of 2.35 μm/s. Analyses of images were carried out using the Nanoscope III software version 5.31R1.

2.2. Preparation of GO nanosheet and GO/DEN–OH/FA

Size-controlled GO nanosheets were prepared by mechanical fracture using an ultrasonic processor. The aqueous dispersion of commercial GO was ultrasonicated in an ice bath for 4 h at an amplitude intensity of 30 and an applied power of 40 W. Afterwards, the GO dispersion was filtrated by using a cellulose acetate membrane filter with a 0.2 μm pore size. The concentration of the obtained GO nanosheets was determined using a calibration curve at an absorption band of 230 nm.

GO/DEN-OH was prepared as shown in Scheme 1 (reaction a) according to the previously reported method [19]. Briefly, an aqueous dispersion (8 cm^3) of GO was centrifuged, and the centrifugate was dispersed in DMF (4 cm^3). A DMF solution (0.4 wt%, 6 cm^3, 90 μM) of the dendrimer was mixed with a DMF solution (4 cm^3) of GO, and esterification of the mixture was facilitated by adding DCC and DMAP for 24 h at room temperature [19]. The product (GO/DEN-OH) was collected, rinsed and re-dispersed in water.

The preparation of GO/DEN-OH/FA (Scheme 1, reaction b) was performed by adding NHS (182.5 mg, 1.6 mmol) and EDC (125 mg, 0.65 mmol) into an aqueous suspension (1 cm^3) of GO/DEN-OH (0.125 mg/ml), and adding an aqueous 10 wt% $NaHCO_3$ solution (pH 8) of FA (0.5 wt%, 9 cm^3, 167 μM) and was stirred for 24 h at room temperature [19]. The product (GO/DEN-OH/FA) was purified by dialysis.

2.3. Loading and release of DOX on GO/DEN-OH/FA

DOX loading onto GO/DEN-OH/FA was carried out as shown in Scheme 1 (reaction c). An aqueous suspension (0.2 cm^3) of GO/DEN-OH/FA (FA = 167 μM) was mixed with DOX (0.8 cm^3) at different DOX concentrations of 8–128 μg/ml and was stirred for 24 h in the dark. Then, the dispersion was dialyzed in a regenerated cellulose tubular membrane (MWCO of 6000–8000 g/mol) against water for 72 h to remove unbound DOX. The amount of unbound DOX in the dialyzed outer solution was determined quantitatively from absorbance at an absorption band (278 nm) of DOX using a calibration curve. The amount of loaded DOX was evaluated by

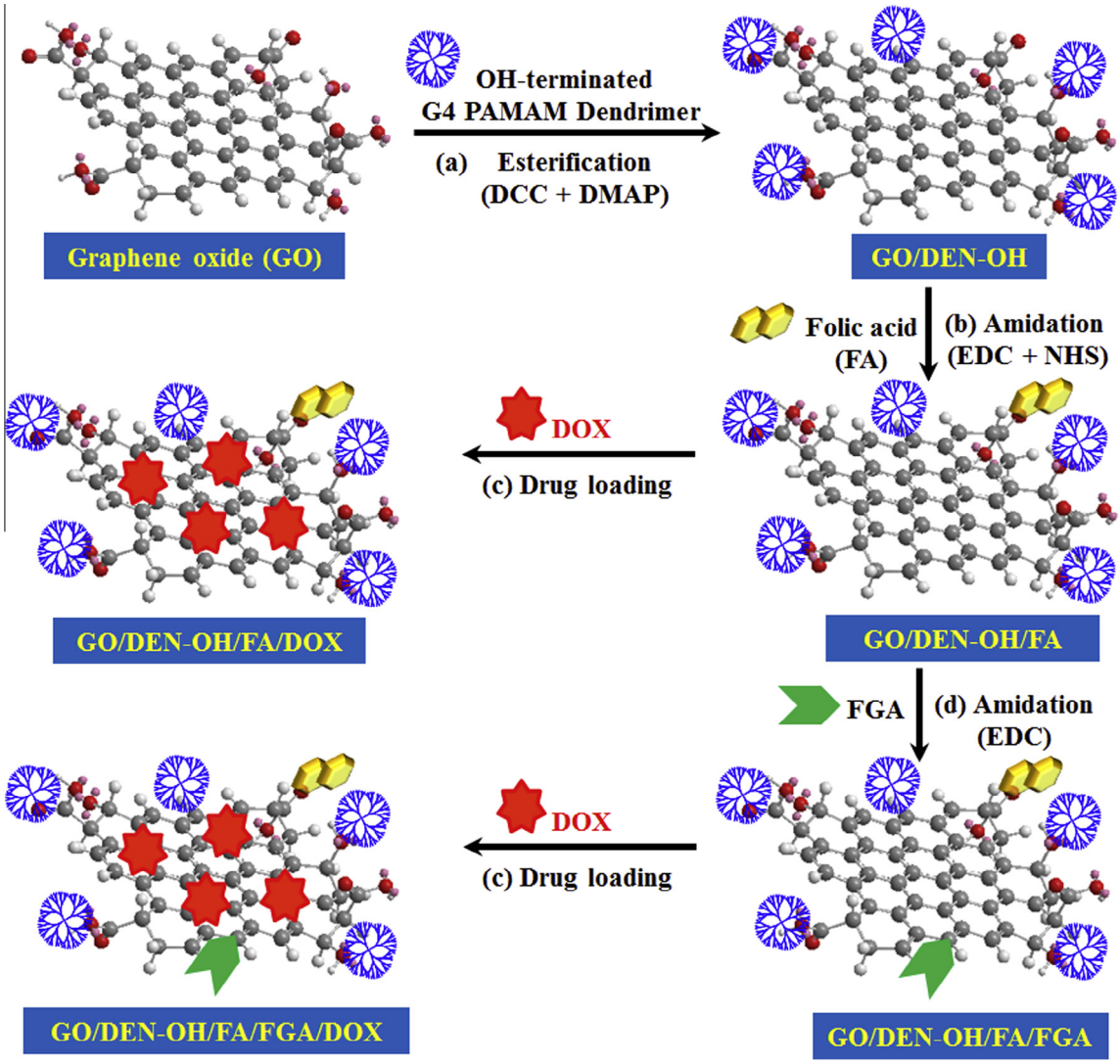

Scheme 1. Schematic illustration of the preparation of GO/DEN-OH/FA/FGA/DOX conjugates.

subtracting the amount of unbound DOX from the initial amount of DOX.

Controlled release of DOX was performed in phosphate buffered solutions (PBSs) at pH 5.5 and 7.4. A suspension of GO/DEN-OH/FA/DOX in a dialysis membrane (MWCO = 3500 g/mol) was dialyzed in 30 cm^3 of water under constant stirring for 72 h at room temperature. The concentration of DOX released into water from GO/DEN-OH/FA was quantified using absorbance at an absorption band of 278 nm.

2.4. In vitro cell viability of GO hybrids

Measurement of in vitro cell viability was performed according to the procedure previously reported [19]. HeLa cells (1×10^4 -cells/well) were grown in DMEM in 96 wells plate for 24 h at 5 vol% CO_2 and 37 °C. Thereafter, the cells were treated with free DOX, GO/DEN-OH/FA/DOX, respectively, at ascending DOX or DOX equivalent concentration (0.01–0.075 μM) to assess the cytotoxicity profiles of GO/DEN-OH/FA/DOX. In addition, Hela cells were also treated with GO/DEN-OH/FA, GO/DEN-OH (carrier control) and blank DMEM (drug control), respectively. Cells were further incubated at 5 vol% CO_2 and 37 °C for 72 h after treatment and the viability of cells was assessed using MTT assay [19].

2.5. Cellular uptake of GO/DEN-OH/FA/DOX

To investigate the targeted uptake of GO/DEN-OH/FA by Hela cells, amine group of FGA (0.26 mM, 2 cm^3) was chemically bound to carboxylic acid group of GO in GO/DEN-OH/FA in an aqueous suspension (2 cm^3) by an amidation reaction, as shown in Scheme 1 (reaction d). Unbound FGA was removed by ultracentrifugation at 13,500 rpm for 1 h. The centrifugate (GO/DEN-OH/FA/FGA) was rinsed three times with water and then re-dispersed in water. The characterizations are given in Supporting Information (Figs. S1 and S4). Subsequently, DOX (20 mg/ml) was loaded onto GO/DEN-OH/FA/FGA (Scheme 1, reaction c). The GO/DEN-OH/FA/FGA/DOX was stored at 4 °C prior to use.

HeLa cells were incubated with GO/DEN-OH/FA/FGA/DOX (0.1 mg/ml) for 2 h. Cells were fixed with 4% paraformaldehyde on a glass plate for 15 min at 37 °C and then rinsed twice with PBS. Then, cell nuclei were stained with Hoechst 33342 (1 μg/ml) for 20 min at room temperature, followed by rinsing with buffer. Cellular uptake of GO/DEN-OH/FA/FGA/DOX was observed by using a CELLOMIC ARRAYSCAN VTI HCS READER (Thermo Scientific). The fluorescence emission of Hoechst 33342 was collected at 461 nm under excitation at 361 nm, and the fluorescence

emission of GO/DEN-OH/FA/FGA/DOX was collected at 515 nm under excitation at 490 nm.

The procedure of flow cytometry is as follows: HeLa cells incubated with GO/DEN-OH/FA/FGA were washed with cold PBS 3 times, followed by Trypsin digestion. Cells were suspended in culture medium for flow cytometric analyses on a flow cytometer equipped with an argon laser (488 nm wavelength). Cell fluorescence was detected in the FL2 channel (wavelength: 585 nm; bandwidth: 42 nm), and the number of positive cells and mean fluorescence intensity were counted.

3. Results and discussion

3.1. Hybridization of DEN-OH, FA and DOX on GO

GO nanosheets were prepared by ultrasonication of commercial GO. The average particle sizes of GO before and after ultrasonication, as measured by DLS, were approximately 1473 and 91 nm, respectively. It is important to note that commercial GO is broken down by the mechanical fracture. Therefore, the commercial GO and ultrasonicated GO nanosheets were named GO_{1500} and GO_{100}, respectively.

DEN-OH and FA were conjugated to GO using condensing agents for esterification and amidation, respectively (Scheme 1). DOX was then loaded onto the GO hybrid (GO/DEN-OH/FA). The morphology of GO, GO/DEN-OH, GO/DEN-OH/FA and GO/DEN-OH/FA/DOX was investigated by TEM, as shown in Fig. 1. The three hybrids exhibited folds or accumulations of GO sheets (darker contrast in TEM images of Fig. 1), which is different from a flat single sheet of GO, although GO_{100} and GO_{100} hybrids are always smaller than GO_{1500} and GO_{1500} hybrids.

Similar morphological variation between GO and GO hybrids was also observed in AFM images (Figs. 2A and 2B). AFM images and their section analyses (Fig. 2A) revealed that GO_{1500} exhibited a large and flat sheet with an average thickness of 2–3 nm and a lateral width of 1–1.5 μm, indicating a few layers of GO sheet. Meanwhile, the thickness of the GO_{100} sheet with 100–150 nm in lateral width was 1 nm, suggesting a single layer. The height evaluated from the height profile of AFM image was 7–30 nm for GO_{1500} hybrids and at most 9 nm for GO_{100} hybrids. The large thickness of GO_{1500} hybrids may come from the promotion of the folding of GO_{1500} derived by the hybridization of DEN-OH and FA. The thickness increase of GO_{100} is rather reasonable, if dendrimers with about 4 nm diameter were immobilized on both surfaces of a GO_{100} sheet. These observations indicate successful immobilization of DEN-OH and FA onto the GO sheets for both hybrids of GO_{1500} and GO_{100}.

The zeta potentials of GO and its hybrids are listed in Table 1. After DEN-OH and FA were conjugated on GO, the negative zeta potential value of GO was decreased, indicating that the number of anionic carboxyl groups on GO was diminished by esterification and amidation with DEN-OH and FA. Moreover, after DOX was loaded onto GO/DEN-OH/FA, the negative zeta potential was further decreased due to the adsorption of DOX onto the GO/DEN-OH/FA surface. Since similar zeta potential values and the same behaviors were obtained between GO_{1500} and GO_{100} and between their hybrids, it can be noted that the surface potential characteristics are almost independent of the size of GO.

The covalent bonding of DEN-OH and FA to GO was then evaluated by infrared (IR) absorption spectroscopy. The IR absorption bands and their locations for each species are shown in Fig. S1 and listed in Table S1. Both GO_{1500} and GO_{100} exhibited IR bands of C=O stretching vibration mode of –COOH group at 1735 cm^{-1} and a CC skeletal vibration mode of graphitic domains at 1622 cm^{-1}, which are similar to previous reports [20,21]. These results indicate that the fragmentation of GO sheets by mechanical fracture do not vary the feature of the graphitic domain of GO. After the conjugation of GO with DEN-OH, the C=O band at 1735 cm^{-1} was significantly weakened or diminished. Meanwhile, new absorption bands of amide I and II vibration modes of DEN-OH at 1627 and 1549 cm^{-1} were observed on the IR spectra of GO/DEN-OH [22]. These observations confirm the covalent binding of DEN-OH to GO through the ester linkage. When FA was conjugated to GO/DEN-OH, the IR absorption spectrum of GO/DEN-OH/FA exhibited a weak band at 1673-1675 cm^{-1}, indicating the successful conjugation of FA to GO/DEN-OH [4,6]. After DOX was loaded onto GO/DEN-OH/FA, the characteristic bands of DOX preferentially appeared at 1722–1724 cm^{-1}, 1613–1615 cm^{-1} and 1578 cm^{-1} [6,23]. This result mentions that DOX was successfully and abundantly loaded onto GO/DEN-OH/FA. These results are consistent with those obtained from AFM. It should also be noted that there are no significant differences between GO_{1500} and GO_{100} hybrids on the IR spectra or in the formation process of the GO/DEN-OH/FA.

Fig. S2 shows Raman spectra of GO and its hybrids under a laser light at 633 nm. GO exhibited Raman D and G bands at 1334–1337 cm^{-1} and 1588–1590 cm^{-1}, respectively. However, the downshift of these bands was observed after the conjugation of DEN-OH and FA and loading of DOX on GO (Table S2), suggesting that there is a perturbation of the vibrational properties of GO. It is well known that the intensity ratio (I_D/I_G) of the D and G Raman bands provides the information about structural defects in carbon materials, such as carbon nanotube and graphene oxide [24,25]. Therefore, it can be implied from Table 1 that the increases in I_D/I_G values of GO/DEN-OH/FA/DOX can be attributed to the increase of defects, owing to the larger degree of functionalization by DEN-OH and FA and loading of DOX on GO.

It was found that GO_{1500} and GO_{100} exhibited the same electronic structure, as shown in Fig. 3. Both GO_{1500} and GO_{100} revealed a main absorption band at 232 nm and a shoulder at around 300 nm, which corresponds to $\pi \rightarrow \pi^*$ transition of aromatic CC bonds and $n \rightarrow \pi^*$ transition of C=O bonds, respectively [8,20]. This indicates that the preparation of GO_{100} by mechanical fracture do not affect to the electronic structure of GO. As shown in Fig. 3, after DEN-OH and FA were bound on GO, absorption bands at 272 and 359 nm indicative of FA were observed, similar to the previous report [19]. In addition, after DOX was loaded onto GO/DEN-OH/FA, the characteristic four intrinsic bands of DOX were observed, indicating the existence of DOX on GO/DEN-OH/FA, as shown in Fig. 3. In addition, an intrinsic absorption band at 482 nm of DOX was obviously shifted to the wavelength approximately 511 nm for GO/DEN-OH/FA was also obvious. This shift might be due to the ground-state electron donor–acceptor interaction between GO/DEN-OH/FA and DOX [4–6,23]. The results from UV–VIS spectroscopy were also consistent with IR results and confirmed successive conjugation of DEN-OH, FA and DOX on GO.

It has been reported that GO/DEN-OH/FA exhibits emission bands at 355 and 450 nm with different intensities at 282 nm excitation (Fig. S3(A)) [19]. Because DOX has a fluorescent hydroxy-substituted anthraquinone chromophore [26], DOX revealed a strong emission band at 560 nm at the excitation wavelength of 500 nm. However, after DOX was loaded onto GO/DEN-OH/FA, fluorescence of DOX was quenched independent of the size of GO, as shown in Fig. S3(B). The fluorescence quenching is the evidence of π–π stacking of DOX on GO/DEN-OH/FA hybrids, similar to the previous reports [26,27].

3.2. Loading and Releasing of DOX on GO/DEN-OH/FA

The amount of drug loading is one of the main parameters to determine the effectiveness of a drug nanocarrier [28]. In the

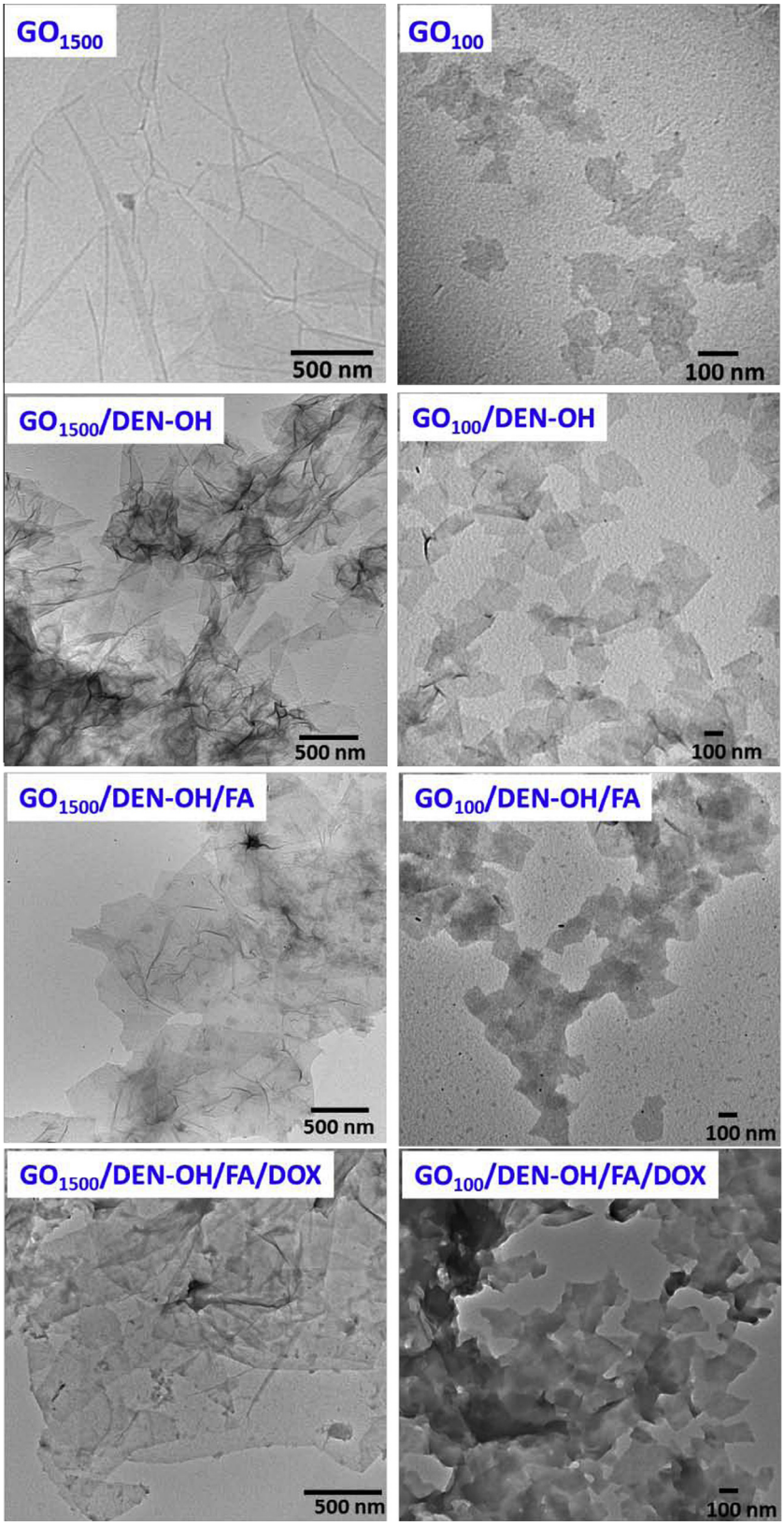

Fig. 1. TEM images of GO, GO/DEN-OH, GO/DEN-OH/FA, and GO/DEN-OH/FA/DOX for both hybrids of GO_{1500} and GO_{100} at GO: DEN-OH: FA = 1: 5: 0.8.

present work, the loading efficiency of GO/DEN-OH/FA was evaluated by using DOX as a representative drug. The amount of DOX loaded on GO/DEN-OH/FA was plotted as a function of DOX concentration in Fig. 4(A). DOX loading onto GO/DEN-OH/FA initially increased with increasing DOX concentration, but it became saturated at concentrations above 0.09 mg/ml. The saturation occurred at 1.83 and 1.43 mg/mg(GO) for GO_{1500} and GO_{100} hybrids, respectively. Importantly, these data mentions that GO_{100}/DEN-OH/FA

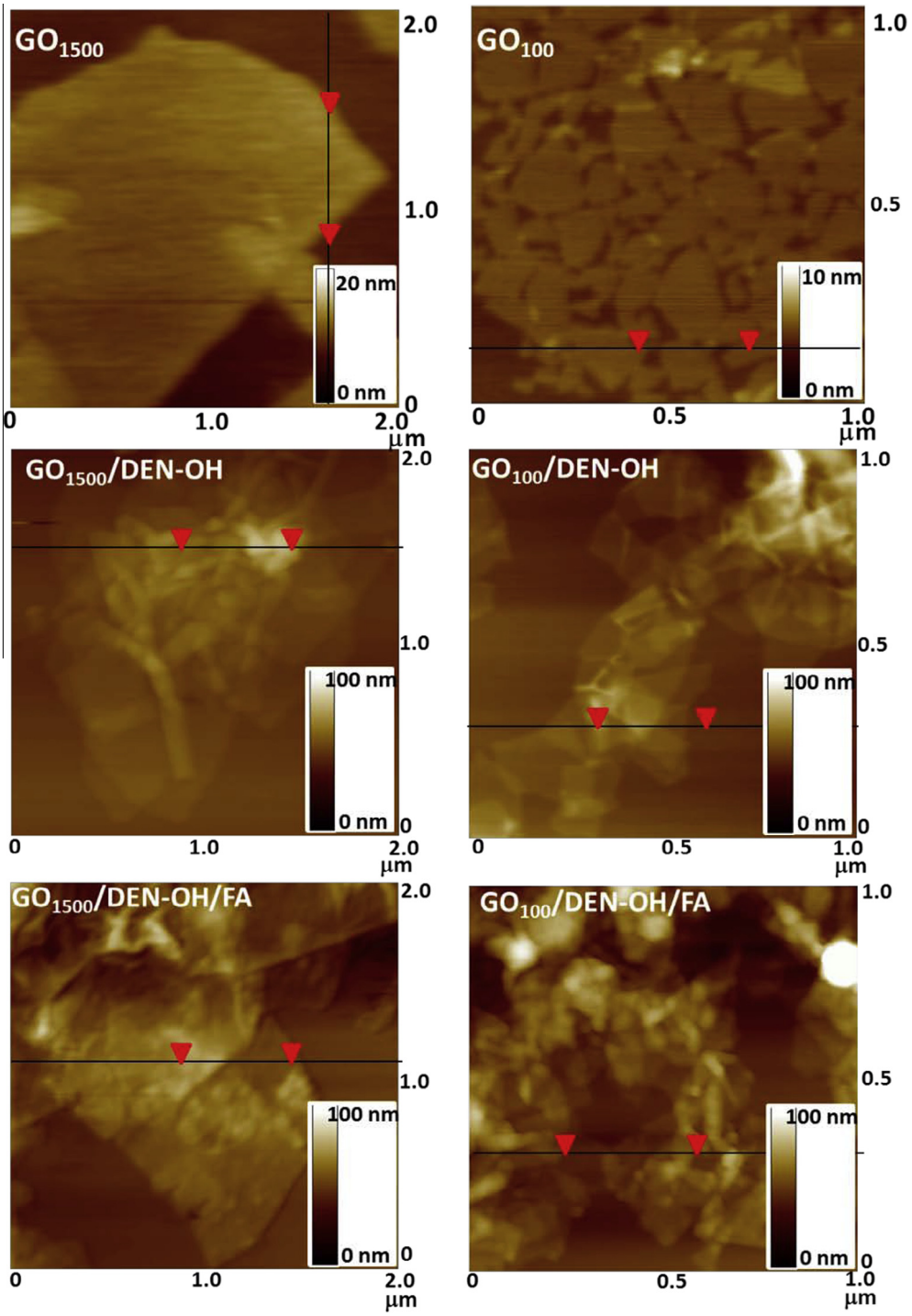

Fig. 2A. AFM images of GO, GO/DEN-OH and GO/DEN-OH/FA for both hybrids of GO_{1500} and GO_{100} at GO: DEN-OH: FA = 1: 5: 0.8. Scan area of GO_{1500} = 2 μm × 2 μm, GO_{100} = 1 μm × 1 μm.

possesses inferior DOX loading efficiency to GO_{1500}/DEN-OH/FA. This might be due to the smaller graphitic domain of GO_{100} compared to GO_{1500}. Generally, DOX can be adsorbed on GO via the π–π stacking interaction between anthraquinone chromophore of DOX and graphitic domain of GO. In addition, amino (NH_2) and hydroxyl (OH) groups of DOX can form the strong hydrogen bonding interaction with OH and COOH groups on GO at neutral pH [3,24,27]. Adsorption profiles in Fig. 4(A) displayed a two-step process before saturation. These steps might be due to the different adsorption interactions described above. It should be noted that even though the surface of GO was partly occupied by DEN-OH and FA, DOX loading on both hybrids of GO_{1500} and GO_{100} is high compared with the other GO nanocarrier systems [3,26]. It has been reported that DOX loading on GO nanosheet is approximately 1 and 2.35 mg/mg(GO) at DOX concentrations of 0.30 [26] and 0.47 [3] mg/ml, respectively. Thus, it can be suggested that the

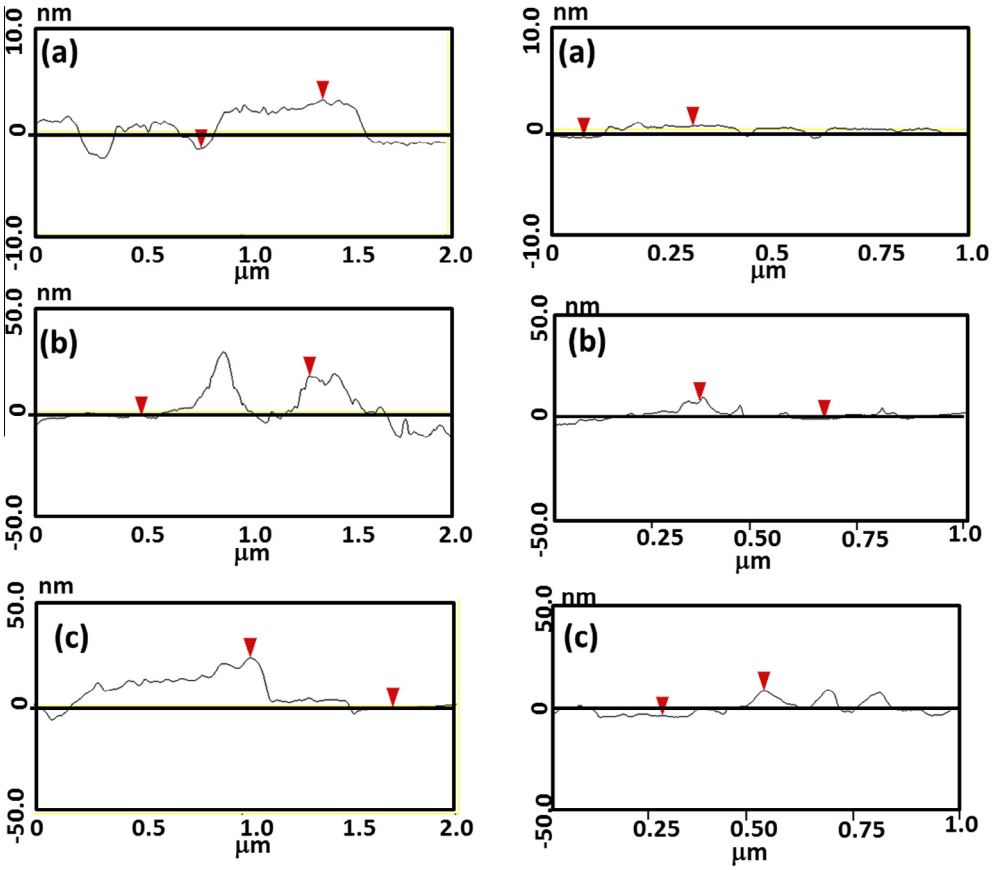

Fig. 2B. Height profiles of AFM images of (a) GO, (b) GO/DEN-OH and (c) GO/DEN-OH/FA for both hybrids of GO_{1500} and GO_{100} at GO: DEN-OH: FA = 1: 5: 0.8.

Table 1
Size (Mean), Z-average and I_D/I_G of GO, GO/DEN-OH, GO/DEN-OH/FA, and GO/DEN-OH/FA/DOX for both hybrid of GO_{1500} and GO_{100}.

Sample	Average mean size (nm)	Average zeta potential (mV)	I_D/I_G
GO_{1500}	1473	−81.4	1.06
GO_{1500}/DEN-OH/FA	537.4	−59.7	1.29
GO_{1500}/DEN-OH/FA/DOX	898.7	−34.2	1.41
GO_{100}	91.4	−79.6	1.07
GO_{100}/DEN-OH/FA	366.8	−51.9	1.61
GO_{100}/DEN-OH/FA/DOX	778.5	−39.9	1.17

occupation of DEN-OH and FA on GO surface does not affect to the loading and stacking of DOX on both GO_{1500}/DEN-OH/FA and GO_{100}/DEN-OH/FA.

Moreover, it has been reported that DOX can also be incorporated inside amine-terminated G4 PAMAM dendrimers (DEN-NH_2) at pH 7.5 (TES buffer) and the amount of DOX loaded was 0.51 mg/mg(DEN-NH_2) [29]. It is also suggested that the hydrophobic interactions between DEN-NH_2 and DOX are favorable at pH 7.5, leading to the increase in the incorporation of DOX inside DEN-NH_2. Therefore, it can be inferred for the case of GO/DEN-OH/FA carriers that DOX could be loaded onto both the unoccupied area of GO surface and also incorporated inside DEN-OH. Importantly, the drug loading capacity of these GO hybrids is higher than that of the other drug carrier materials such as carbon nanotube (0.5–0.6 mg/mg(carbon nanotube)) [30] and polymer vesicles (0.47 mg/mg(polymer)) [31]. Generally, drug loading capacities of the common drug carriers are lower than 1 mg/mg(carrier) at the saturated carrying concentration [26]. Taken together, these data suggest that GO/DEN-OH/FA carriers are promising potential drug carriers.

In the present work, the releasing of DOX from GO/DEN-OH/FA was investigated at pH 5.5 and 7.4 to be mimic tumor environment and physiological pH in body fluid, respectively [32]. As seen in Fig. 4(B), DOX releasing is pH-dependent with superior release observed at pH 5.5 compared to pH 7.4. At pH 7.4, the releasing from GO/DEN-OH/FA after 72 h is approximately 26% (15.6 μg/ml) and 35% (18.9 μg/ml) for GO_{1500} and GO_{100}, respectively. At pH 5.5, the releasing amount reached 75% (45 μg/ml) and 86% (46.4 μg/ml), for GO_{1500} and GO_{100}, respectively, which are almost 3-fold high to those at pH 5.5 in DOX releasing. At pH 5.5, the protonation of NH_2 groups on DOX can break the hydrogen bonding with COOH on GO/DEN-OH/FA, leading to the release of DOX from GO/DEN-OH/FA [3,6]. These data suggest that DOX should be released from GO/DEN-OH/FA in the tumor cells, because the tumor cells are more acidic (pH 5.5) than the normal tissues (pH 7.4). Moreover, these data show that a greater amount of DOX is released from GO_{100}/DEN-OH/FA than GO_{1500}/DEN-OH/FA, which might be due to the smaller graphitic domain and subsequent weak interaction between DOX and GO_{100}/DEN-OH/FA. Additionally, full release at pH 5.5 is attained after 30–40 h, which should provide a large window of time for drug delivery to the appropriate tissues.

3.3. In vitro cell viability

The cell viability of GO, GO hybrids and free DOX was investigated by MTT assay with HeLa cells, as shown in Fig. 5. MTT results revealed that the viability was highly dependent on carrier concentration. This result is similar to the previous report that the GO/FA carriers exhibit dose-dependent toxicity [33]. The viability of Hela

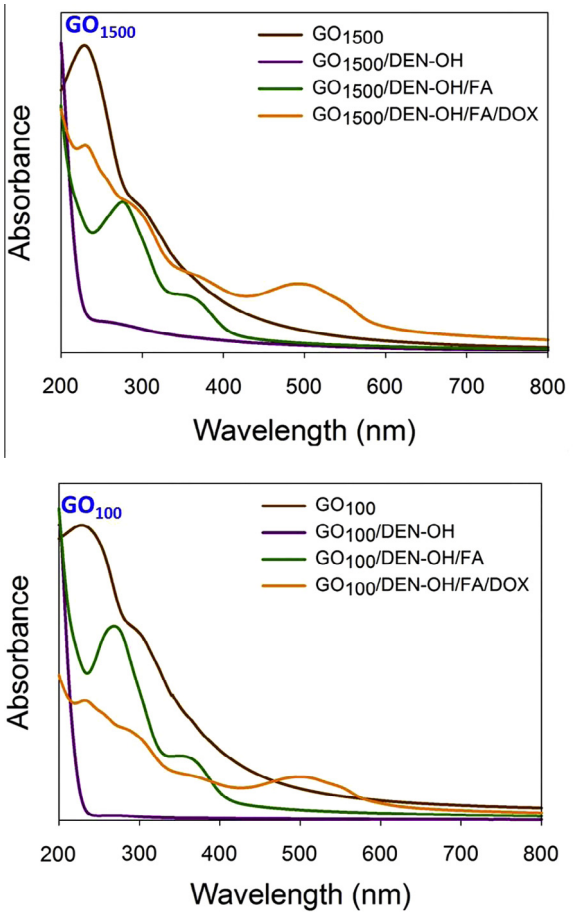

Fig. 3. UV–visible absorption spectra of GO, GO/DEN-OH, GO/DEN-OH/FA and GO/DEN-OH/FA/DOX for both GO_{1500} and GO_{100}.

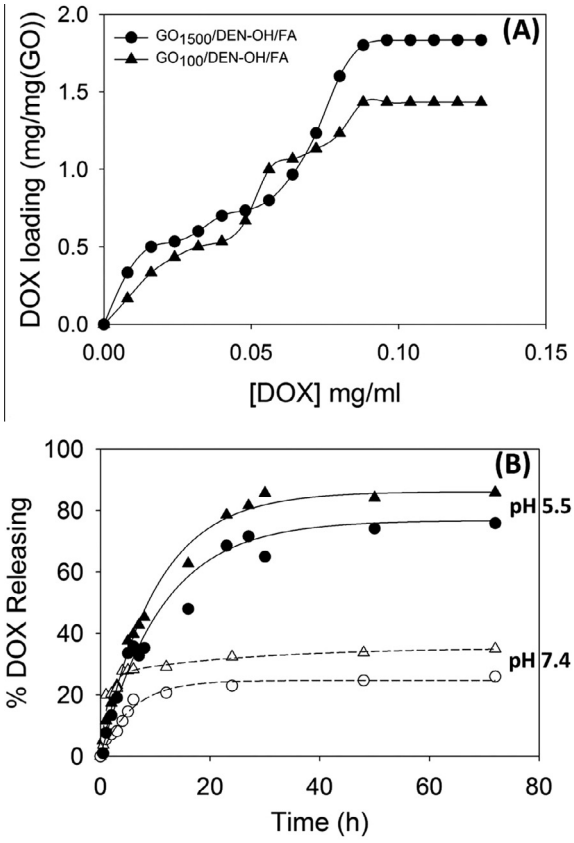

Fig. 4. (A) DOX loading and (B) releasing at pH 5.5 and 7.4 on GO/DEN-OH/FA for both hybrids of GO_{1500} (●○) and GO_{100} (▲△).

cells remained 75%, when the cells were incubated with 0.75 μg/ml of GO_{100}, while the cell viability was decreased to 64% at 0.75 μg/ml of GO_{1500}. This indicates that GO_{100} exhibits less cytotoxicity towards HeLa cells than GO_{1500}. These results are inconsistent with a previous report on A549 cells, which stated that the viability was lowered after incubation with 160 nm-sized GO compared to 780 nm-sized GO (67% vs 80%) [34].This inconsistency is most likely due to the difference in the synthesis and preparation of GO or in the type of cells.

Moreover, MTT results indicated that the covalent binding of DEN-OH to GO decreased cell viability, which was further exacerbated by the hybridization of FA on GO/DEN-OH. It should be noted that the tendency towards decreased viability was less for GO_{100} hybrids than GO_{1500} hybrids. These results reveal that GO_{100}/DEN-OH hybrids are less cytotoxic than GO_{1500}/DEN-OH hybrids, similar to the relation of GO_{1500} and GO_{100} as described above. The increased cytotoxicity of GO hybrids is most likely due to the enhanced cell membrane-penetrating effect of the dendrimer towards HeLa cells. Further, it has been reported that the cytotoxicity of carbon-based materials significantly increases, when the number of COOH and/or OH groups is increased on the surface of carbon-based materials [12,35].

It has been suggested that the conjugation of FA to GO hybrid, GO/Fe_3O_4/DOX, provides the selective killing of cancer cells in vitro [6,36,37]. Therefore, the increase in the cytotoxicity from GO/DEN-OH to GO/DEN-OH/FA observed in these studies might be due to the presence of FA on the GO hybrids. Additionally, the viability towards HeLa cells was significantly high for GO_{100}/DEN-OH/FA at 0.75 μg/ml compared to GO_{1500}/DEN-OH/FA at the same concentration (63% vs 31%), which is consistent with the size effect of GO hybrids outlined above.

After DOX was loaded onto GO/DEN-OH/FA, the MTT results showed a significant increase in cell death compared to unloaded control. As expected, GO_{100}/DEN-OH/FA/DOX exhibited less cytotoxicity than GO_{1500}/DEN-OH/FA/DOX. It is well known that DOX is highly toxic for HeLa cells [6,36,37], and so the increased cytotoxicity of GO/DEN-OH/FA/DOX can likely be attributed to DOX. It has previously been reported that FA-nano-GO loading with two anticancer drugs displayed specific targeting to MCF-7 cells and remarkably high cytotoxicity as compared to nano-GO loading with only either DOX or CPT [4].

3.4. Cellular targeting uptake of GO_{100}/DEN-OH/FA/FGA

In consideration of enhanced permeability and retention (EPR) effect [38], cellular uptake of GO_{100}/DEN-OH/FA/DOX within targeted cells was investigated using fluorescence microscopy, since GO_{100}/DEN-OH/FA/DOX is an adequate anticancer drug delivery system with enough small size to satisfy the EPR effect. In the fluorescence images, HeLa nuclei were stained in blue (Hoechst 33342), while FGA-conjugated GO/DEN-OH/FA were displayed in green, as shown in Fig. 6. The characteristic green fluorescence of FGA bound to GO_{100}/DEN-OH/FA/DOX was observed in HeLa cells, suggesting the uptake of GO_{100}/DEN-OH/FA/DOX by cells. This implies that GO_{100}/DEN-OH/FA/DOX can be effectively delivered into the targeted tumor cells, i.e., into HeLa cells that highly express the folate receptor. The internalized GO_{100}/DEN-OH/FA/DOX was mainly localized in the cytoplasm and not inside the nucleus, suggesting that GO_{100}/DEN-OH/FA/DOX is able to penetrate the cell membrane.

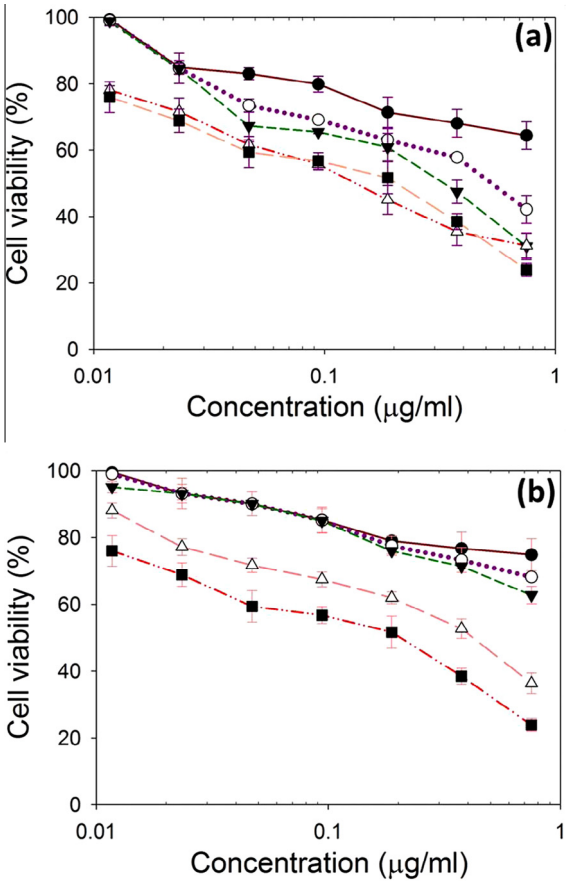

Fig. 5. Cell viability as a function of DOX concentration. (●) GO, (○) GO/DEN-OH, (▼) GO/DEN-OH/FA, (△) GO/DEN-OH/FA/DOX and (■) DOX for both hybrids of (a) GO_{1500} and (b) GO_{100}.

Flow cytometry with laser irradiation at 488 nm was carried out to quantify the cellular uptake efficiency of GO_{100}/DEN-OH/FA/FGA for HeLa cells. These experiments allowed for a determination of the number of GO/DEN-OH/FA/FGA positive cells and the average fluorescence intensity per cell [18]. The flow histograms shown in Fig. 7 indicated that more than 97% of GO_{100}/DEN-OH/FA was internalized at the concentration of 62.5 μg/ml, and the efficient uptake for the GO_{100}/DEN-OH/FA hybrid was observed even at 31.25 and 15.6 μg/ml. Namely, the results indicate that the GO_{100}/DEN-OH/FA hybrid can be efficiently taken up by HeLa cells, while GO_{100} alone (control) was scarcely taken up by HeLa cells. In addition, whereas the presence of FA resulted in high uptake of GO/DEN-OH/FA, there were even the low uptakes of GO/DEN-OH. This fact obviously indicates that folic acid-conjugated hybrid can be effectively delivered into the targeted tumor cells, i.e., into HeLa cells that have high expression to folate receptor [39,40]. However, it must be noticed that GO/DEN-OH hybrid also can be taken up by Hela cells due to the cellular targeting ability of DEN-OH, although it is weaker than that of FA. Both fluorescence and flow cytometric observations support the potential for GO/DEN-OH/FA hybrid materials to be used as drug nanocarriers in biological systems.

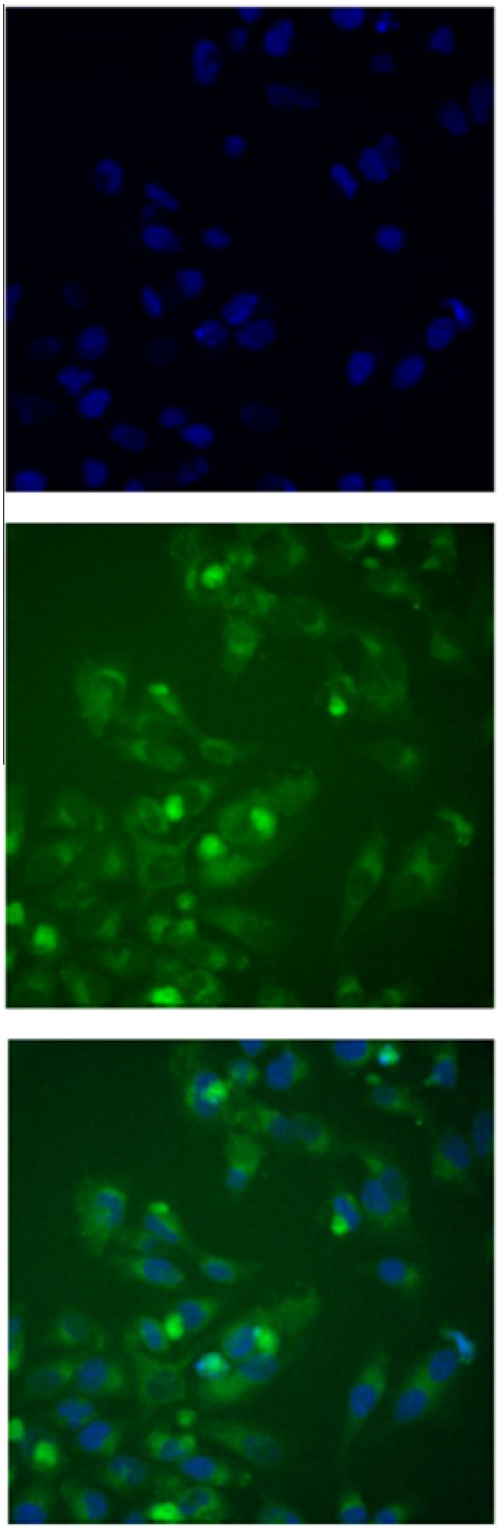

Fig. 6. Fluorescence images of HeLa cells with GO_{100}/DEN-OH/FA/FGA/DOX (0.1 mg/ml).

4. Conclusions

Hybrid materials (GO/DEN-OH/FA) of GO with fourth generation DEN-OH and FA were successfully prepared. It was found that GO_{100}/DEN-OH/FA possessed a lower DOX loading capacity than GO_{1500}/DEN-OH/FA, although the loading amount of 1.43 mg/mg(GO) for GO_{100} hybrid was enough high in comparison of conventional drug delivery systems. This might be due to the size of the graphitic domain of GO_{100}/DEN-OH/FA, which was smaller than the domain of the GO_{1500}/DEN-OH/FA hybrids. However, the amount of DOX released from GO_{100}/DEN-OH/FA was greater than that from GO_{1500}/DEN-OH/FA. This was

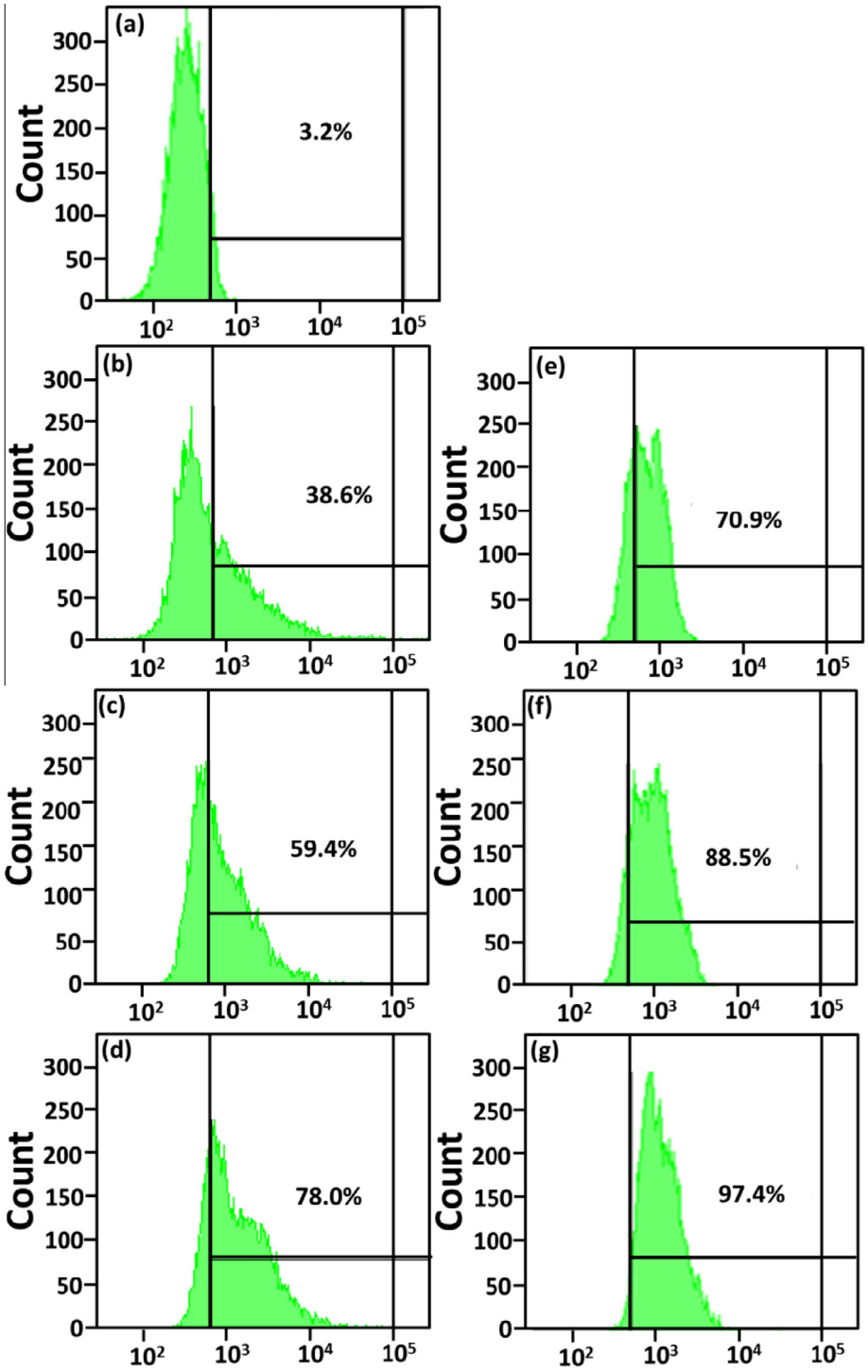

Fig. 7. Flow histograms of (a) GO_{100}/FGA, (b–d) GO_{100}/DEN-OH/FGA and (e–g) GO_{100}/DEN-OH/FA/FGA at concentrations of GO_{100} or its hybrids at (a) 62.5 mg/ml, (b,e) 15.6 mg/ml, (c,f) 31.25 mg/ml, and (d,g) 62.5 mg/ml.

particularly true at pH 5.5, where the amount of DOX released was 86%, and complete release occurred slowly over the course of approximately 40 h.

MTT results revealed that GO_{100} hybrids exhibit less cytotoxicity than GO_{1500} hybrids. Incidentally, the cell viability was higher than 63% for GO_{100}, GO_{100}/DEN-OH and GO_{100}/DEN-OH/FA at 0.75 μg/ml. In addition, GO/DEN-OH/FA/DOX displayed an ability to kill HeLa cells with both hybrids of GO_{1500} and GO_{100}. This effect is likely due to the conjugation of DEN-OH and FA, which enhances cell membrane-penetration and the selective targeting of HeLa cells, respectively. Lastly, the studies demonstrated efficient internalization of DOX-loaded GO_{100}/DEN-OH/FA/DOX into HeLa cells with high uptake amount (97% at 62.5 mg/ml). These observations support the potential for GO/DEN-OH/FA hybrid materials to be used as drug nanocarriers in biological systems.

Acknowledgments

This bilateral cooperation program was supported by the Malaysia Ministry of Higher Education's HIR-MOHE Grants

(UM.C/625/1/HIR/MOHE/MED/17 and UM.C/625/1/HIR/MOHE/MED/33). A.S. gratefully acknowledges the National Science Council of Taiwan for the award of the Postdoctoral Fellowship (NSC 102-2221-E-011-114). We also thank Prof. H.C. Tsai of National Taiwan University of Science and Technology for his kind support for the cell viability experiments.

Appendix A. Supplementary data

Supplementary data associated with this article can be found, in the online version, at http://dx.doi.org/10.1016/j.cej.2015.07.024.

References

[1] Z.Y. Zhang, Y.D. Xu, Y.Y. Ma, L.L. Qiu, Y. Wang, J.L. Kong, H.M. Xiong, Biodegradable ZnO@polymer core–shell nanocarriers: pH-triggered release of doxorubicin in vitro, Angew. Chem. Int. Ed. 52 (2013) 4127.
[2] X. Hu, X. Hao, Y. Wu, J. Zhang, X. Zhang, P.C. Wang, G. Zou, X.J. Liang, Multifunctional hybrid silica nanoparticles for controlled doxorubicin loading and release with thermal and pH dual response, J. Mater. Chem. B 1 (2013) 1109.
[3] X. Yang, X. Zhang, Z. Liu, Y. Ma, Y. Huang, Y. Chen, High-efficiency loading and controlled release of doxorubicin hydrochloride on graphene oxide, J. Phys. Chem. C 112 (2008) 17554.
[4] L. Zhang, J. Xia, Q. Zhao, L. Liu, Z. Zhang, Functional graphene oxide as a nanocarrier for controlled loading and targeted delivery of mixed anticancer drugs, Small 6 (2010) 537.
[5] Y. Yang, Y.M. Zhang, Y. Chen, D. Zhao, J.T. Chen, Y. Liu, Construction of a graphene oxide based noncovalent multiple nanosupramolecular assembly as a scaffold for drug delivery, Chem. Eur. J. 18 (2012) 4208.
[6] X. Yang, Y. Wang, X. Huang, Y. Ma, Y. Huang, R. Yang, H. Duana, Y. Chen, Multi-functionalized graphene oxide based anticancer drug-carrier with dual-targeting function and pH-sensitivity, J. Mater. Chem. 21 (2011) 3448.
[7] G. Wei, M. Yan, R. Dong, D. Wang, X. Zhou, J. Chen, J. Hao, Covalent modification of reduced graphene oxide by means of diazonium chemistry and use as a drug-delivery system, Chem. Eur. J. 18 (2012) 14708.
[8] X. Sun, Z. Liu, K. Welsher, J.T. Robinson, A. Goodwin, S. Zaric, H. Dai, Nano-graphene oxide for cellular imaging and drug delivery, Nano Res. 1 (2008) 203.
[9] K.S. Novolov, A.K. Geim, S.V. Morozov, D. Jiang, Y. Zhang, S.V. Dubonos, I.V. Grigorieva, A.A. Firsov, Electric field effect in atomically thin carbon films, Science 306 (2004) 666.
[10] K. Wang, J. Ruan, H. Song, J. Zhang, Y. Wo, S. Guo, D. Cui, Nanoscale. Biocompatibility of graphene oxide. Nanoscale, Res. Lett. 6 (2011) 1.
[11] Z. Liu, J.T. Robinson, X. Sun, H. Dai, J. Am. Chem. Soc. 130 (2008) 10876.
[12] P.S. Wate, S.S. Banerjee, A. Jalota-Badhwar, R.R. Mascarenhas, K.R. Zope, J. Khandare, R.D.K. Misra, PEGylated nano-graphene oxide for delivery of water insoluble cancer drugs, Nanotechnology 23 (2012) 415101.
[13] R. Duncan, L. Izzo, Dendrimer biocompatibility and toxicity, Adv. Drug Delivery Rev. 57 (2005) 2215.
[14] S.C. Medina, M.E.H. El-Sayed, Dendrimers as carriers for delivery of chemotherapeutic agents, Chem. Rev. 109 (2009) 3141.
[15] X.F. Li, T. Imae, D. Leisner, M.A. López-Quintela, Lamellar structures of anionic poly(amido amine) dendrimers with oppositely charged didodecyldimethylammonium bromide, J. Phys. Chem. B 106 (2002) 12170.
[16] V. Tiriveedhi, K.M. Kitchens, K.J. Nevels, H. Ghandehari, P. Butko, Kinetic analysis of the interaction between poly(amidoamine) dendrimers and model lipid membranes, Biochim. Biophys. Acta 1808 (2011) 209.
[17] J.J. Khandare, S. Jayant, A. Singh, P. Chandna, Y. Wang, N. Vorsa, T. Minko, Dendrimer versus linear conjugate: influence of polymeric architecture on the delivery and anticancer effect of paclitaxel, Bioconj. Chem. 17 (2006) 1464.
[18] Y.J. Tsai, C.C. Hu, C.C. Chu, T. Imae, Intrinsically fluorescent PAMAM dendrimer as gene carrier and nanoprobe for nucleic acids delivery: bioimaging and transfection study, Biomacromolecules 12 (2011) 4238.
[19] A. Siriviriyanun, T. Imae, G. Calderó, C. Solans, Phototherapeutic functionality of biocompatible graphene oxide/dendrimer hybrids, Colloids Surf. B Biointerfaces 121 (2014) 469.
[20] J.I. Paredes, S. Villar-Rodil, A. Martinez-Alonso, J.M.D. Tascon, Graphene oxide dispersions in organic solvents, Langmuir 24 (2008) 10560.
[21] D. Yu, Y. Yang, M. Durstock, J.B. Baek, L. Dai, Soluble P3HT-grafted graphene for efficient bilayer-heterojunction photovoltaic devices, ACS Nano 4 (2010) 5633.
[22] X. Lu, T. Imae, Dendrimer-mediated synthesis of water-dispersible carbon-nanotubes-supported oxide nanoparticles, J. Phys. Chem. C 111 (2007) 8459.
[23] X.C. Qin, Z.Y. Guo, Z.M. Liu, W. Zhang, M.M. Wan, B.W. Yang, Folic acid-conjugated graphene oxide for cancer targeted chemo-photothermal therapy, J. Photochem. Photobiol. B 120 (2013) 156.
[24] F. Buffa, H. Hu, D.E. Resasco, Side-wall functionalization of single-walled carbon nanotubes with 4-hydroxymethylaniline followed by polymerization of ε-caprolactone, Macromolecules 38 (2005) 8258.
[25] B.J. Olade, M. Aizpurua, A. Garcia, I. Bustero, I. Obieta, M.J. Jurado, Single-walled carbon nanotubes and multiwalled carbon nanotubes functionalized with poly(l-lactic acid): a comparative study, J. Phys. Chem. C 112 (2008) 10663.
[26] D. Depan, J. Shah, R.D.K. Misra, Controlled release of drug from folate-decorated and graphene mediated drug delivery system: synthesis, loading efficiency, and drug release response, Mater. Sci. Eng., C 31 (2011) 1305.
[27] S.P. Sherlock, S.M. Tabakman, L. Xie, H. Dai, Photothermally enhanced drug delivery by ultrasmall multifunctional FeCo/graphitic shell nNanocrystals, ACS Nano 5 (2011) 1505.
[28] H.Q. Hu, J.H. Yu, Y.Y. Li, J. Zhao, H.Q. Dong, Engineering of a novel pluronic F127/graphene nanohybrid for pH responsive drug delivery, J. Biomed. Mater. Res. B 100A (2012) 141.
[29] A. Papagiannaros, K. Dimas, G.T. Papaioannou, C. Demetzos, Doxorubicin-PAMAM dendrimer complex attached to liposomes: cytotoxic studies against human cancer cell lines, Int. J. Pharm. 302 (2005) 29.
[30] Z. Liu, X. Sun, N. Nakayama-Ratchford, H. Dai, Supramolecular chemistry on water-soluble carbon nanotubes for drug loading and delivery, ACS Nano 1 (2007) 50.
[31] C. Sanson, C. Schatz, J.F. Le Meins, A. Soum, J. Thévenot, E. Garanger, S. Lecommandoux, A simple method to achieve high doxorubicin loading in biodegradable polymersomes, J. Control. Release 147 (2010) 428.
[32] S. Kayal, R.V. Ramanujan, Doxorubicin loaded PVA coated iron oxide nanoparticles for targeted drug delivery, Mater. Sci. Eng., C 30 (2010) 484.
[33] P. Huang, C. Xu, J. Lin, C. Wang, X. Wang, C. Zhang, X. Zhou, S. Guo, D. Cui, Folic acid-conjugated graphene oxide loaded with photosensitizers for targeting photodynamic therapy, Theranotics 1 (2011) 240.
[34] Y. Chang, S.T. Yang, J.H. Liu, E. Dong, Y. Wang, A. Cao, Y. Liu, H. Wang, In vitro toxicity evaluation of graphene oxide on A549 cells, Toxicol. Lett. 200 (2011) 301.
[35] A. Magrez, S. Kasas, V. Salicio, N. Pasquier, J.W. Seo, M. Celio, S. Catsicas, B. Schwaller, L. Forro, Cellular toxicity of carbon-based nanomaterials, Nano Lett. 6 (2006) 1121.
[36] X. Yang, G. Niu, X. Cao, Y. Wen, R. Xiang, H. Duan, Y. Chen, The preparation of functionalized graphene oxide for targeted intracellular delivery of SiRNA, J. Mater. Chem. 22 (2012) 6649.
[37] C. Wang, L. Cheng, Z. Liu, Drug delivery with upconversion nanoparticles for multi-functional targeted cancer cell imaging and therapy, Biomaterials 32 (2011) 1110.
[38] K. Greish, Enhanced permeability and retention (EPR) effect for anticancer nanomedicine drug targeting, Methods Mol. Biol. 624 (2010) 25.
[39] L. Li, J. Liu, Z. Diao, D. Shu, P. Guo, G. Shen, Evaluation of specific delivery of chimeric phi29 pRNA/siRNA nanoparticles to multiple tumor cells, Mol. BioSyst. 5 (2009) 1361.
[40] D. Feng, Y. Song, W. Shi, X. Li, H. Ma, Distinguishing folate-receptor-positive cells from folate-receptor-negative cells using a fluorescence off–on nanoprobe, Anal. Chem. 85 (13) (2013) 6530.